

Three dimensional Free Vibration and Transient Analysis of Two Directional Functionally Graded Thick Cylindrical Panels Under Impact Loading

Abstract

In this paper three dimensional free vibration and transient response of a cylindrical panel made of two directional functionally graded materials (2D-FGMs) based on three dimensional equations of elasticity and subjected to internal impact loading is considered. Material properties vary through both radial and axial directions continuously. The 3D graded finite element method (GFEM) based on Rayleigh-Ritz energy formulation and Newmark direct integration method has been applied to solve the equations in space and time domains. The fundamental normalized natural frequency, time history of displacements and stresses in three directions and velocity of radial stress wave propagation for various values of span angle of cylindrical panel and different power law exponents have been investigated. The present results show that using 2D-FGMs leads to a more flexible design than conventional 1D-FGMs. The GFEM solution have been compared with the results of an FG thick hollow cylinder and an FG curved panel, where a good agreement between them is observed.

Keywords

Dynamic Analysis, Impact Loading, Cylindrical Panel, Theory of Elasticity, 2D Functionally Graded Materials, Graded Finite Element Method

Hassan Zafarmand ^a

Manouchehr Salehi ^b

Kamran Asemi ^c

^a Mechanical Engineering Department, Amirkabir University of Technology, Tehran, Iran.

(Permanent Address: Department of Mechanical Engineering, Ferdowsi University of Mashhad, Mashhad, Iran.)

Ha.zafarmand@stu.um.ac.ir

^b Mechanical Engineering Department, Amirkabir University of Technology, Tehran, Iran.

Msalehi@aut.ac.ir

^c Mechanical Engineering Department, Amirkabir University of Technology, Tehran, Iran.

Kamiran64@yahoo.com

<http://dx.doi.org/10.1590/1679-78251099>

Received 06.11.2013

In revised form 17.07.2014

Accepted 01.10.2014

Available online 13.10.2014

1 INTRODUCTION

In recent years, the composition of several different materials is often used in structural components in order to optimize the responses of structures subjected to thermal and mechanical loads. Functionally graded materials (FGMs) are suitable to achieve this purpose. FGMs are composite materials, microscopically inhomogeneous, in which the mechanical properties vary smoothly and continuously from one surface to the other. This idea was used for the first time by Japanese researchers (Koizumi, 1993), which led to the concept of FGMs.

Cylindrical panels are of practical interest in many fields of engineering, including civil, mechanical, and aerospace, as they give rise to optimum conditions for dynamic behavior. The dynamic loadings on these structures can have serious consequences for their strength and safety. Many papers studying FGMs have been published recently. A critical literature review of these works is presented by Birman and Byrd (2007) and Jha *et al.* (2013). Also, a wide range of researches has been carried out on dynamic analysis of FGM structures (Qian *et al.*, 2004; Asemi *et al.*, 2010; Akbarzadeh *et al.*, 2011; Sun and Luo, 2011; Malekzadeh and Monajjemzadeh, 2013; Uymaz and Aydogdu, 2007) which mostly use the plate and shell theories. Among the FGM structures, little attention has been given to analysis of FGM cylindrical structures than those of rectangular and circular ones. For example, Shakeri *et al.* (2006) presented the vibration and radial wave propagation velocity in an FG thick hollow cylinder under dynamic loading by dividing the cylinder into some homogeneous sub-cylinders. Hosseini *et al.* (2007) studied the dynamic responses and natural frequencies of an infinite FG cylinder under internal pressure. Asgari *et al.* (2009) studied the dynamic behavior of a 2D-FG thick hollow cylinder with finite length under impact loading. Asemi *et al.* (2011) investigated the dynamic behavior and radial wave propagation of thick short length FG cylinders. Shao *et al.* (2004; 2005) analytically obtained the elastic behavior of finite length FG hollow cylinders with simply supported end conditions under the hydrostatic pressures. In these publications, in order to satisfy the boundary conditions, the sinusoidal load along the axial direction can only be used. Bodaghi and Shakeri (2012) by using Hamilton's principle and first order shear deformation theory (FSDT) studied the free vibration and dynamic response of simply supported FG piezoelectric cylindrical panel impacted by time-dependent blast pulses. Yas and Sobhani Aragh (2010) investigated the three dimensional steady state response of an FG fiber reinforced orthotropic cylindrical panel simply supported at the radial edges. Wang and Sudak (2008) presented a general method for the analysis of a thermoelastic multi-layered cylindrical panel made of an oblique pile of FG layers having orthotropic material properties. The two edges of the panel are simply-supported. Bahtui and Eslami (2007) studied the coupled thermoelastic response of an FG axisymmetric cylindrical shell. A second order shear deformation shell theory and Galerkin finite element formulation are used to formulate the problem. Davar *et al.* (2013) investigated the response of simply supported circular cylindrical shell made of FGM subjected to lateral impulse load. First order shear deformation theory and Love's first approximation theory are utilized in the equilibrium equations. Qu *et al.* (2013) studied vibrational response of FG shells of revolution with arbitrary boundary conditions. The formulation is derived by means of a modified variational principle in conjunction with a multi-segment partitioning procedure on the basis of the first-order shear deformation shell theory. Ebrahimi and Najafizadeh (2014) analyzed the free vibration of a 2F-FG circular cylindrical shell.

The equations of motion are based on the Love's first approximation classical shell theory and the equations of motion and boundary conditions are discretized by the methods of generalized differential quadrature (GDQ) and generalized integral quadrature (GIQ).

The literature review denotes that most of the studies deal with axisymmetric FG cylindrical shells and they are based on the shear deformation theories. The application of these theories to thick structures can cause considerable errors. Therefore, for eliminating the lack of these studies, the 3D elasticity solutions not only provides realistic and accurate results but also allows further physical insights, which cannot otherwise be estimated by the other two dimensional or plate and shell theories. Also, in these studies, the material properties are assumed to have a smooth variation usually in one direction and majority of researches works into static analyses. Investigations into dynamic analysis of FG cylindrical structures are limited to one and two dimensional analyses. Also, analytical or semi-analytical solutions are available only through a number of problems with simple boundary conditions or for cylindrical panels with simply supported radial edges. Moreover, conventional functionally graded materials may also not be so effective in such design problems since all outer surface of the body will have the same composition distribution. Therefore, variation of volume fraction in two directions has a higher capability to reduce the mechanical, thermal and residual stresses and leads to a more flexible design than 1D-FGMs. Some studies have been carried out about static and dynamic analyses of structures made of 2D-FGMs (Asgari and Akhlaghi, 2010; Nemat-Allah, 2009; Zafarmand and Hassani, 2014).

Due to difficulty in obtaining analytical solutions for dynamic analysis of 2D-FG cylindrical panel based on 3D elasticity and for arbitrary boundary conditions, powerful numerical methods such as graded finite element method (GFEM) are needed. The graded finite elements, which incorporate the material property gradient at the size scale of the element, have been employed a generalized isoparametric formulation. Some works can be found in the literature on modeling nonhomogeneous structures by using GFEM (Kim and Paulino, 2009; Ashrafi *et al.*, 2012; Zafarmand and Kadkhodayan, 2014). In these studies, it is shown that the conventional FEM formulation cause a discontinuous stress field in the direction perpendicular to the material property gradation, while the graded elements give a continuous and smooth variation. However, when the loading is parallel to the material gradation direction, the GFEM formulation estimates sharp rises in stress at the element boundaries while the conventional FEM formulation does not.

To the best knowledge of the authors, there are no studies available in the literature on dynamic analysis of 2D-FG cylindrical panel with clamped boundary conditions based on 3D elasticity and graded finite elements. The governing equations are derived based on principle of minimum potential energy and Rayleigh-Ritz method. To solve the time dependent equations, Newmark direct integration method with suitable time steps has been used. The effects of volume fraction exponents and different span angles on the time histories of displacements, stresses, velocities of radial stress wave propagation and fundamental normalized natural frequency have been investigated.

2 PROBLEM FORMULATION

2.1 Volume fraction and material distribution in 2D-FG cylindrical panel

A functionally graded cylindrical panel with inner radius a , outer radius b , length L and span angle β subjected to an internal impact loading is considered. The geometry and coordinate system of the cylindrical panel is shown in Figure 1.

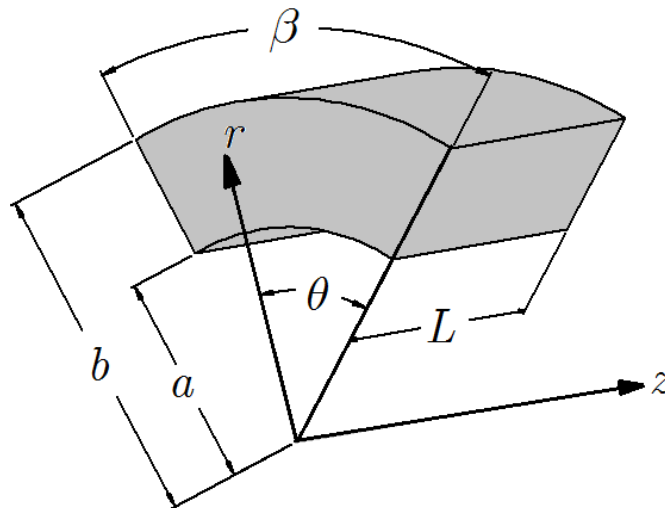


Figure 1: Geometry of the cylindrical panel

2D-FGMs are usually made by continuous gradation of three or four different material phases where one or two of them are ceramics and the others are metal alloy phases. Significant developments in fabrication and processing methods have made it possible to produce FGMs with two and three dimensional gradients using computer aided manufacturing processes. Therefore, the inner surface of the cylindrical panel is made of two distinct ceramics and the outer surface of two metals. The volume fractions of the constituent materials vary continuously through radial and axial directions in a predetermined composition profile. The volume fraction distribution function of each material can be expressed as:

$$V_{c1}(r, z) = \left[1 - \left(\frac{r - a}{b - a} \right)^{n_r} \right] \left[1 - \left(\frac{z}{L} \right)^{n_z} \right] \quad (1)$$

$$V_{c2}(r, z) = \left[1 - \left(\frac{r - a}{b - a} \right)^{n_r} \right] \left(\frac{z}{L} \right)^{n_z} \quad (2)$$

$$V_{m1}(r, z) = \left(\frac{r - a}{b - a} \right)^{n_r} \left[1 - \left(\frac{z}{L} \right)^{n_z} \right] \quad (3)$$

$$V_{m2}(r, z) = \left(\frac{r - a}{b - a} \right)^{n_r} \left(\frac{z}{L} \right)^{n_z} \tag{4}$$

where $c1$, $c2$, $m1$ and $m2$ denote first ceramic, second ceramic, first metal and second metal, respectively. n_r and n_z are non-negative volume fraction exponents through the r and z directions. For instant, the volume fraction distributions of the first metal (V_{m1}) for the typical values of $n_r = n_z = 3$ is shown in Figure 2. In this case $a = 0.2\text{ m}$, $b = 0.4\text{ m}$ and $L = 1\text{ m}$. According to this figure, V_{m1} is equal to one at $r = b, z = 0$ and equal to zero at other corners and its variation in $r - z$ plane depends on n_r and n_z . Similarly V_{m2} , V_{c1} and V_{c2} are equal to one at $r = b, z = L$, $r = a, z = 0$ and $r = a, z = L$, respectively.

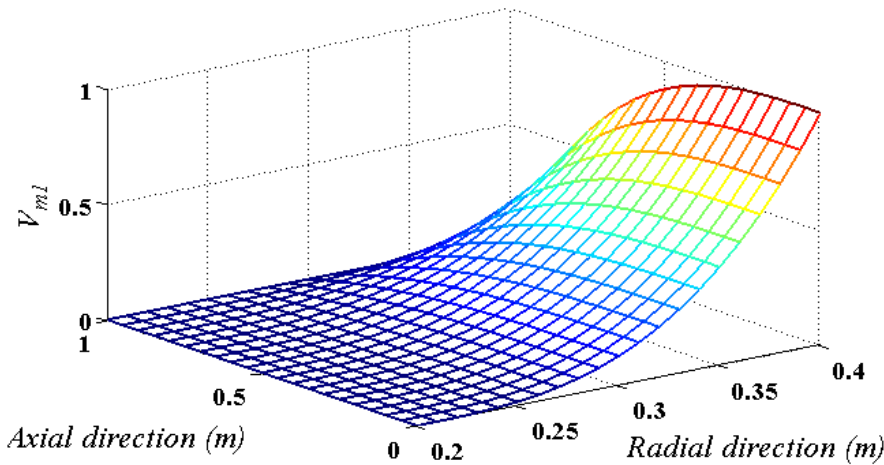


Figure 2: Volume fraction distribution of $m1$ with $n_r = n_z = 3$

Material properties at each point can be obtained by using the linear rule of mixtures, therefore the material property (\mathfrak{R}) such as modulus of elasticity and mass density in the 2D-FG cylindrical panel is determined by linear combination of volume fractions and material properties of the basic materials as:

$$\mathfrak{R} = \mathfrak{R}_{c1}V_{c1} + \mathfrak{R}_{c2}V_{c2} + \mathfrak{R}_{m1}V_{m1} + \mathfrak{R}_{m2}V_{m2} \tag{5}$$

Accordingly, the cylindrical panel is pure $c1$, $c2$, $m1$ and $m2$ at $r = a, z = 0$, $r = a, z = L$, $r = b, z = 0$ and $r = b, z = L$, respectively and the variation of desired material property depends on the volume fraction distributions of the constituents in which the volume fractions depends on n_r and n_z . For example, the variation of a material property such as modulus of elasticity based on the mentioned approach for the typical values of $n_r = n_z = 3$ is shown in Figure 3. As it can

be seen from this figure, the elastic modulus is equal to E_{c1} , E_{c2} , E_{m1} and E_{m2} at $r = a, z = 0$, $r = a, z = L$, $r = b, z = 0$ and $r = b, z = L$, respectively and varies in $r - z$ plane based on Eq. (5). The volume fractions in Eqs. (1-4) reduce to the conventional 1D-FGMs for $n_z = 0$ and in this case, the material properties vary only through the thickness direction. The basic constituents of the 2D-FG cylindrical panel are presented in Table 1. It should be noted that Poisson's ratio is assumed to be a constant value of 0.3. This assumption is reasonable because of the small differences between the Poisson's ratios of basic materials.

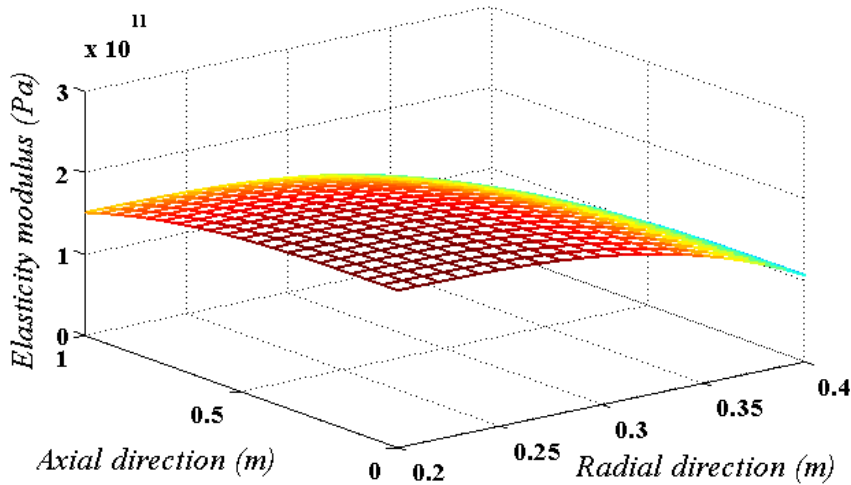


Figure 3: Distribution of elasticity modulus with $n_r = n_z = 3$

Constituents	Material	E (GPa)	ρ (kg/m ³)
$m1$	Ti6A14V	105.7	4429
$m2$	Al 1,100	70	2707
$c1$	MnO	193	5026
$c2$	ZrO ₂	151	3000

Table 1: Basic constituents of the 2D-FG cylindrical panel

2.2 Governing Equations

Neglecting body forces, the equations of motion in cylindrical coordinates are obtained as:

$$\frac{\partial \sigma_r}{\partial r} + \frac{1}{r} \frac{\partial \sigma_{r\theta}}{\partial \theta} + \frac{\partial \sigma_{rz}}{\partial z} + \frac{\sigma_r - \sigma_\theta}{r} = \rho(r, z) \frac{\partial^2 u}{\partial t^2} \tag{6-1}$$

$$\frac{\partial \sigma_{r\theta}}{\partial r} + \frac{1}{r} \frac{\partial \sigma_\theta}{\partial \theta} + \frac{\partial \sigma_{\theta z}}{\partial z} + \frac{2\sigma_{r\theta}}{r} = \rho(r, z) \frac{\partial^2 v}{\partial t^2} \tag{6-2}$$

$$\frac{\partial \sigma_{rz}}{\partial r} + \frac{1}{r} \frac{\partial \sigma_{\theta z}}{\partial \theta} + \frac{\partial \sigma_z}{\partial z} + \frac{\sigma_{rz}}{r} = \rho(r, z) \frac{\partial^2 w}{\partial t^2} \quad (6-3)$$

where u , v and w are radial, circumferential and axial components of displacement, respectively and ρ is the mass density that depends on r and z coordinates.

The stress-strain relations from the Hook's law in the matrix form are as:

$$\boldsymbol{\sigma} = \mathbf{D}\boldsymbol{\varepsilon} \quad (7)$$

where the stress and strain components and the coefficients of elasticity \mathbf{D} , are as the following relations:

$$\boldsymbol{\sigma} = \{\sigma_r \quad \sigma_\theta \quad \sigma_z \quad \sigma_{\theta z} \quad \sigma_{rz} \quad \sigma_{r\theta}\}^T \quad (8)$$

$$\boldsymbol{\varepsilon} = \{\varepsilon_r \quad \varepsilon_\theta \quad \varepsilon_z \quad \gamma_{\theta z} \quad \gamma_{rz} \quad \gamma_{r\theta}\}^T \quad (9)$$

$$\mathbf{D} = \frac{E(r, z)}{(1 + \nu)(1 - 2\nu)} \begin{bmatrix} 1 - \nu & \nu & \nu & 0 & 0 & 0 \\ \nu & 1 - \nu & \nu & 0 & 0 & 0 \\ \nu & \nu & 1 - \nu & 0 & 0 & 0 \\ 0 & 0 & 0 & \frac{1 - 2\nu}{2} & 0 & 0 \\ 0 & 0 & 0 & 0 & \frac{1 - 2\nu}{2} & 0 \\ 0 & 0 & 0 & 0 & 0 & \frac{1 - 2\nu}{2} \end{bmatrix} \quad (10)$$

where ν denotes the Poisson's ratio and E is the Young's modulus of elasticity that depends on r and z coordinates.

The strain-displacement equations based on the theory of linear elasticity in cylindrical coordinate are:

$$\begin{aligned} \varepsilon_r &= \frac{\partial u}{\partial r} \quad , \quad \gamma_{\theta z} = \frac{\partial v}{\partial z} + \frac{1}{r} \frac{\partial w}{\partial \theta} \\ \varepsilon_\theta &= \frac{1}{r} \left(u + \frac{\partial v}{\partial \theta} \right) \quad , \quad \gamma_{rz} = \frac{\partial u}{\partial z} + \frac{\partial w}{\partial r} \\ \varepsilon_z &= \frac{\partial w}{\partial z} \quad , \quad \gamma_{r\theta} = \frac{1}{r} \frac{\partial u}{\partial \theta} + \frac{\partial v}{\partial r} - \frac{v}{r} \end{aligned} \quad (11)$$

and in the matrix form are as:

$$\boldsymbol{\varepsilon} = \mathbf{L}\mathbf{U} \quad (12)$$

where \mathbf{U} is the displacements vector and \mathcal{L} is a matrix containing partial differentiating equations as:

$$\mathbf{U} = \{u \quad v \quad w\}^T \quad (13)$$

$$\mathcal{L} = \begin{bmatrix} \partial_r & 1/r & 0 & 0 & \partial_z & 1/r \partial_\theta \\ 0 & 1/r \partial_\theta & 0 & \partial_z & 0 & \partial_r - 1/r \\ 0 & 0 & \partial_z & 1/r \partial_\theta & \partial_r & 0 \end{bmatrix}^T \quad (14)$$

The cylindrical panel is clamped on its two end edges and it is subjected to internal pressure that is a function of time. Therefore, the boundary conditions are as:

$$\mathbf{U}|_{z=0,L} = 0 \quad (15)$$

The internal pressure function $p_r(t)$ is an arbitrary function that will be presented later.

2.3 Graded finite element modeling

In order to solve the governing equations the graded finite element method is used. In this method, in addition to displacement field, the heterogeneity of the material properties of the FGM may also be determined based on their nodal values. In this regard, shape functions similar to those of the displacement field may be used. This procedure can be used even for multi-directional functionally graded materials. Therefore, a graded finite element method (GFEM) is used to effectively trace smooth variations of the material properties at the element level. Using the graded elements for modeling of gradation of the material leads to more accurate results than dividing the solution domain into homogenous elements.

The cylindrical panel is divided into a number of 8-node linear elements. For element (e), the displacements in three directions are approximated as follow:

$$\mathbf{U}^{(e)} = \mathbf{\Phi} \mathbf{\Lambda}^{(e)} \quad (16)$$

where $\mathbf{\Phi}$ is the matrix of linear shape functions in cylindrical coordinate and $\mathbf{\Lambda}^{(e)}$ is the nodal displacement vector of the element that are as:

$$\mathbf{\Phi} = \begin{bmatrix} \Phi_1 & 0 & 0 & \dots & \Phi_8 & 0 & 0 \\ 0 & \Phi_1 & 0 & \dots & 0 & \Phi_8 & 0 \\ 0 & 0 & \Phi_1 & \dots & 0 & 0 & \Phi_8 \end{bmatrix} \quad (17)$$

$$\mathbf{\Lambda}^{(e)} = \{U_1 \quad V_1 \quad W_1 \quad \dots \quad U_8 \quad V_8 \quad W_8\}^T \quad (18)$$

the components of $\mathbf{\Phi}$ are given in the appendix.

To treat the material inhomogeneity by using the GFEM, it may be written:

$$\boldsymbol{\Psi}^{(e)} = \sum_{i=1}^8 \boldsymbol{\Psi}_i \Phi_i \quad (19)$$

where $\boldsymbol{\Psi}^{(e)}$ is the material property of the element.

Substituting Eq. (16) in Eq. (12) gives the strain matrix of element (e) as:

$$\boldsymbol{\varepsilon}^{(e)} = \mathbf{B}\boldsymbol{\Lambda}^{(e)} \quad (20)$$

where:

$$\mathbf{B} = \mathcal{L}\boldsymbol{\Phi}^{(e)} \quad (21)$$

Now by using Hamilton's principal and Rayleigh-Ritz energy formulation, the GFEM is imposed and finally the mass, stiffness and force matrices are obtained as following:

$$\int_{t_1}^{t_2} \delta(\Pi - T - W)dt = 0 \quad (22)$$

where Π , T and W are potential energy, kinetic energy and virtual work done by surface tractions, respectively. These functions and their variations are:

$$\Pi = \frac{1}{2} \iiint_V \boldsymbol{\varepsilon}^T \boldsymbol{\sigma} dV \quad (23)$$

$$\delta\Pi = \iiint_V \delta\boldsymbol{\varepsilon}^T \boldsymbol{\sigma} dV \quad (24)$$

$$T = \frac{1}{2} \iiint_V \rho \dot{\mathbf{U}}^T \dot{\mathbf{U}} dV \quad (25)$$

$$\delta T = \iiint_V \rho \dot{\mathbf{U}}^T \delta \dot{\mathbf{U}} dV \quad (26)$$

$$W = \iint_A \mathbf{P}^T \mathbf{U} dA \quad (27)$$

$$\delta W = \iint_A \mathbf{P}^T \delta \mathbf{U} dA \quad (28)$$

where V and A are the volume and area of the domain under consideration and \mathbf{P} is the vector of surface traction and in the case of internal pressure is as:

$$\mathbf{P} = \{p_r \quad 0 \quad 0\}^T \quad (29)$$

Substituting Eqs. (23-28) in Hamilton's Principal, applying side conditions $\delta U|_{t_1, t_2} = 0$ and using part integration:

$$\iiint_V \delta \varepsilon^T \sigma dV + \iiint_V \rho \ddot{U}^T \delta U dV = \iint_A \mathbf{P}^T \delta U dA \quad (30)$$

For each element, by imposing Eqs. (7, 16 and 20) into Eq. (30), it can be achieved:

$$\begin{aligned} \delta \mathbf{A}^{(e)T} \left\{ \iiint_V \rho \Phi^T \Phi dV \right\} \ddot{\mathbf{A}}^{(e)} + \delta \mathbf{A}^{(e)T} \left\{ \iiint_V \mathbf{B}^T \mathbf{D} \mathbf{B} dV \right\} \mathbf{A}^{(e)} \\ = \delta \mathbf{A}^{(e)T} \iint_A \Phi^T \mathbf{P} dA \end{aligned} \quad (31)$$

Since $\delta \mathbf{A}^{(e)T}$ is the variation of the nodal displacements and is arbitrary, it can be omitted from Eq. (31), thus this equation can be written as:

$$\mathbf{M}^{(e)} \ddot{\mathbf{A}}^{(e)} + \mathbf{K}^{(e)} \mathbf{A}^{(e)} = \mathbf{F}^{(e)} \quad (32)$$

where the characteristic matrices are defined as:

$$\mathbf{M}^{(e)} = \iiint_V \rho \Phi^T \Phi dV \quad (33)$$

$$\mathbf{K}^{(e)} = \iiint_V \mathbf{B}^T \mathbf{D} \mathbf{B} dV \quad (34)$$

$$\mathbf{F}^{(e)} = \iint_A \Phi^T \mathbf{P} dA \quad (35)$$

As \mathbf{D} and ρ are not constant, for obtaining the characteristic matrices for each element, numerical integration should be applied.

Now by assembling the element matrices and imposing the boundary conditions, the global equations of motion for the 2D-FG cylindrical panel can be written as:

$$\mathbf{M} \ddot{\mathbf{A}} + \mathbf{K} \mathbf{A} = \mathbf{F} \quad (36)$$

Once the finite element equations are determined, for free vibration analysis where the force matrix (\mathbf{F}) is zero, by substituting $\mathbf{A} = \mathbf{A}_0 e^{i\omega t}$ (ω is the natural frequency) into Eq. (36), an eigen value problem would be obtained that can be solved using standard eigen value extraction procedures. Also, in the case of transient analysis, the Newmark direct integration method with suitable time steps is utilized to solve the equations. Newmark integration parameters are taken as (Zienkiewicz and Taylor, 2005):

$$\gamma_{Newmark} = 1/2, \quad \beta_{Newmark} = 1/4 \quad (37)$$

which lead to a constant average acceleration. This choice of parameters corresponds to a trapezoidal rule which is unconditionally stable in linear analyzes.

3 NUMERICAL RESULTS AND DISCUSSION

3.1 Validation

To validate the transient analysis of the current work, the data of an FG thick hollow cylinder under internal impact loading can be used (Asemi et al., 2011). Material distribution is assumed to be as 1D-FGM and it varies in radial direction with a power law function. In order to validate the results of this paper with the results of the present study, the span angel of the panel should be taken 2π to become a hollow cylinder, n_z is taken zero, $a = 1\text{ m}$, $b = 1.5\text{ m}$, $L = 1\text{ m}$, $E_{m2} = 70\text{ GPa}$, $\rho_{m2} = 2707\text{ kg/m}^3$, $E_{c2} = 380\text{ GPa}$, $\rho_{c2} = 3800\text{ kg/m}^3$ and the internal loading function is assumed to be as:

$$p_r(t) = \begin{cases} P_0 t & t \leq 0.005\text{ s} \\ 0 & t > 0.005\text{ s} \end{cases} \quad (38)$$

where P_0 is 4 GPa/s . The comparison of the radial displacement at $r = 1.25\text{ m}$ and $z = 0.5\text{ m}$ for $n_r = 0.5$ with the published data is shown in Figure 4 and a good agreement between these two results is observed.

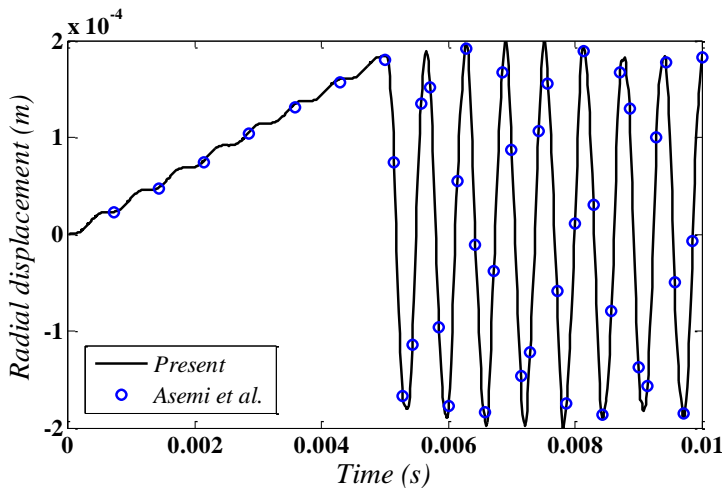


Figure 4: Time history of the radial displacement at $r = 1.25\text{ m}$ and $z = 0.5\text{ m}$ for $n_r = 0.5$ compared with (Asemi et al., 2011)

Also, in order to validate the free vibration analysis of this study, the data of an FG curved panel can be used (Zahedinejad, 2010). The material properties are assumed to be varied from ceramic ($E_c = 380\text{ GPa}$, $\rho_c = 3800\text{ kg/m}^3$) at inner radius to metal ($E_m = 70\text{ GPa}$, $\rho_m = 2702\text{ kg/m}^3$) at

outer radius with a power law function. The boundary conditions are simply supported in four edges and the geometry is defined as:

$$\begin{aligned} a &= 0.75 \text{ m} \quad , \quad L = 1 \text{ m} \\ b &= 1.25 \text{ m} \quad , \quad \beta = 1 \text{ rad} \end{aligned} \quad (39)$$

The comparison of fundamental frequency parameter ($\bar{\omega} = \omega(b-a)\sqrt{\rho_c/E_c}$) with the published results for different power law exponents is made in Table 2. According to this table, a closed agreement between the present results and those obtained from Zahedinejad (2010) is observed.

	n_r					
	0	0.5	1	4	10	∞
Present	0.8612	0.7523	0.6798	0.5407	0.4902	0.4453
Zahedinejad (2010)	0.8675	0.7578	0.6870	0.5475	0.4940	0.4496
Difference (%)	0.7	0.7	1	1.2	0.8	0.9

Table 2: The fundamental frequency parameter for FG cylindrical panel with four edges simply supported compared with (Zahedinejad, 2010)

3.3 Numerical Results

Consider a 2D-FG cylindrical panel with inner radius $a = 0.2 \text{ m}$, outer radius $b = 0.4 \text{ m}$ and length of $L = 0.5 \text{ m}$. The panel is clamped at $z = 0, L$ and subjected to an impact loading at its inner surface. Constituent materials are two distinct ceramics and two distinct metals described in Table 1. The Poisson's ratio is taken as a constant value of 0.3 and the loading function is assumed to be as:

$$p_r(t) = \begin{cases} P_0 \sin(\pi t/t_0) & t \leq t_0 \\ 0 & t > t_0 \end{cases} \quad (40)$$

where P_0 and t_0 are loading constants that are assumed to be as 10^7 Pa and $5 \times 10^{-4} \text{ s}$, respectively. Variation of the internal pressure with time is displayed in Figure 5. According to this figure, the cylindrical panel is excited by unloading in $t_0 = 5 \times 10^{-4} \text{ s}$. It is obvious that after the unloading, a transient vibration which is affected by the wave propagation, reflection and interference would be occurred. The three dimensional transient and free vibration analysis for different values of the power law exponents and span angles are presented and discussed as following.

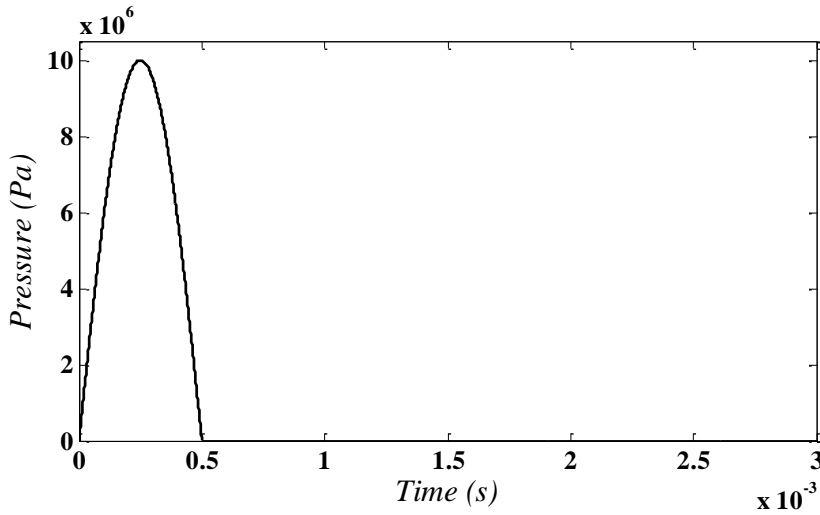


Figure 5: Variation of internal pressure (p_r) with time.

Figures 6 and 7 show the time history of radial displacement at $r = 0.3\text{ m}$, $\theta = 30^\circ$, $z = 0.25\text{ m}$ and $r = 0.35\text{ m}$, $\theta = 15^\circ$, $z = 0.125\text{ m}$, respectively after the unloading for different values of the power law exponents. The span angle of the cylindrical panel is assumed to be $\beta = \pi/3$. These figures denote that the maximum amplitude of vibration belongs to the panel with power law exponents of $n_r = 0$, $n_z = 3$. In this case the cylinder is made of first and second metal and the material distribution vary through the axial direction only. Also it can be seen from this figures that the minimum amplitude of vibration is for $n_r = 3$, $n_z = 3$.

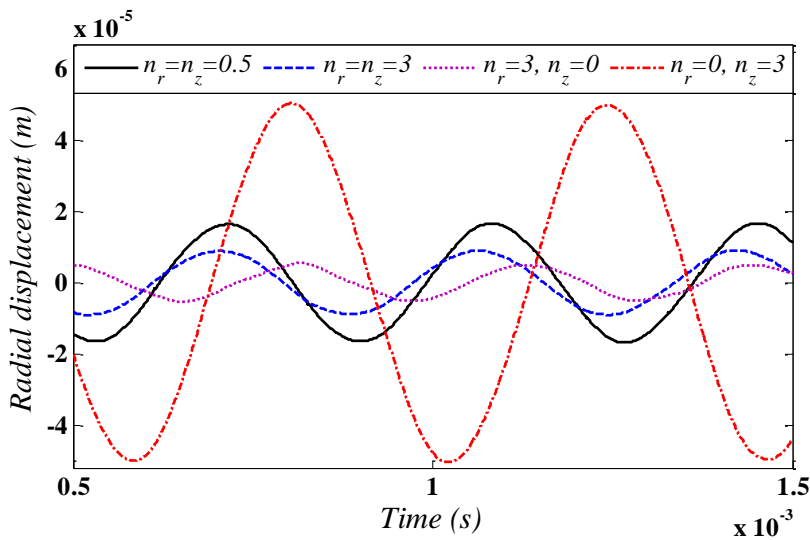


Figure 6: Time history of the radial displacement at $r = 0.3\text{ m}$, $\theta = 30^\circ$, $z = 0.25\text{ m}$ with $\beta = \pi/3$ for different values of n_r and n_z

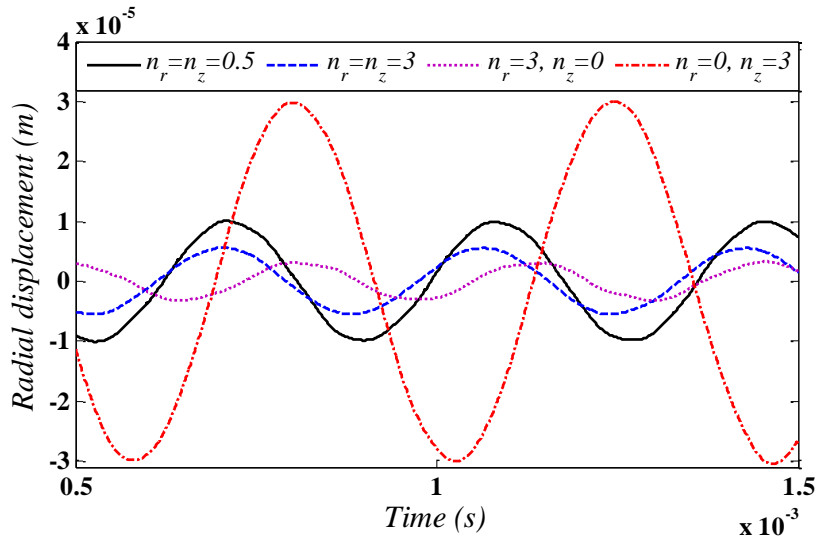


Figure 7: Time history of the radial displacement at $r = 0.35 m$, $\theta = 15^\circ$, $z = 0.125 m$ with $\beta = \pi/3$ for different values of n_r and n_z

The time history of circumferential displacement at $r = 0.25 m$, $\theta = 45^\circ$, $z = 0.375 m$ for a cylindrical panel with $\beta = \pi/3$ after the unloading for different values of power law exponent is demonstrated in Figure 8. According to this figure, due to asymmetry of geometry, the circumferential displacement cannot be neglected. These results show how the time histories of displacements field are affected by the variation of volume fraction of constituent materials in two directions.

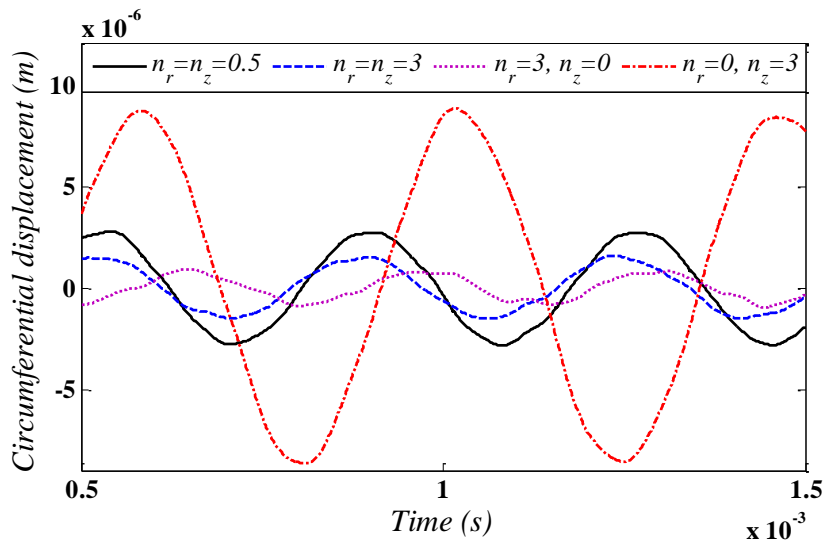


Figure 8: Time history of the circumferential displacement at $r = 0.25 m$, $\theta = 45^\circ$, $z = 0.375 m$ with $\beta = \pi/3$ for different values of n_r and n_z

The time history of radial, circumferential, shear ($\sigma_{r\theta}$) and axial stresses, respectively at $r = 0.3\text{ m}$, $\theta = 30^\circ$, $z = 0.25\text{ m}$ for a cylindrical panel with $\beta = \pi/3$ after the unloading for different values of power law exponent are shown in Figures 9-12. It is obvious that variation of stresses is highly dependent of power law exponents. Also, as the same as circumferential displacement, the shear stress ($\sigma_{r\theta}$) cannot be neglected in asymmetric geometries.

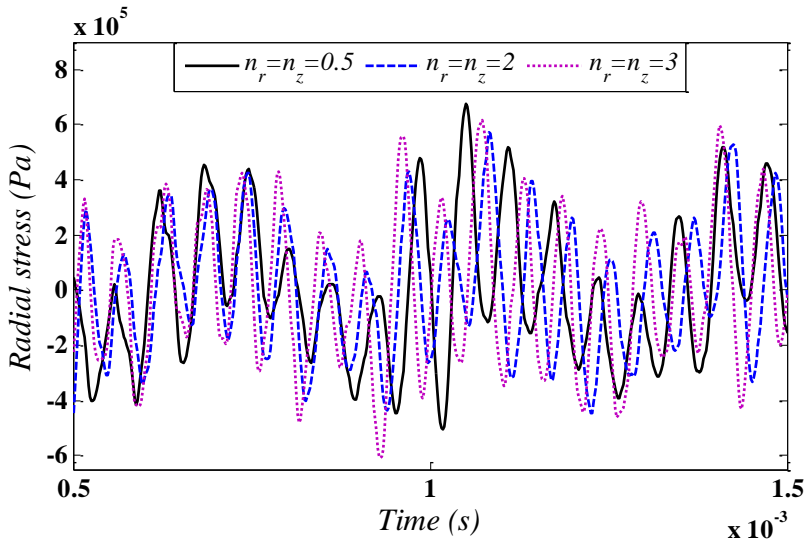


Figure 9: Time history of the radial stress at $r = 0.3\text{ m}$, $\theta = 30^\circ$, $z = 0.25\text{ m}$ with $\beta = \pi/3$ for different values of n_r and n_z

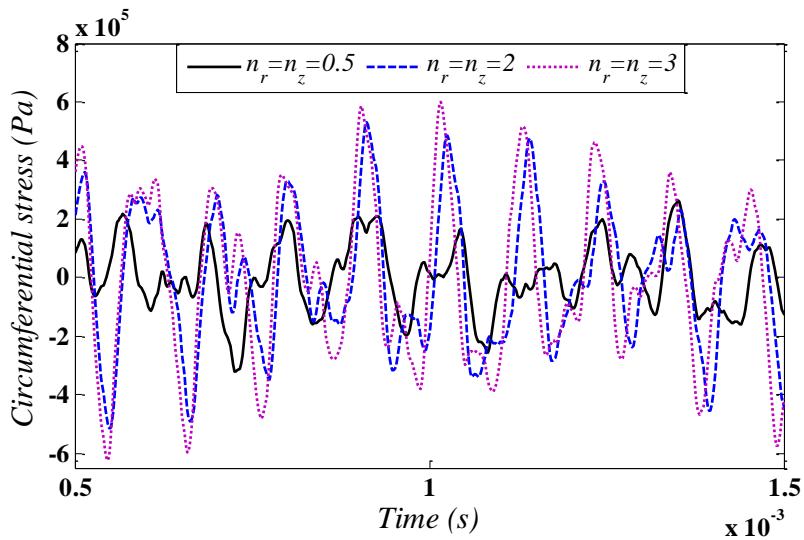


Figure 10: Time history of the circumferential stress at $r = 0.3\text{ m}$, $\theta = 30^\circ$, $z = 0.25\text{ m}$ with $\beta = \pi/3$ for different values of n_r and n_z

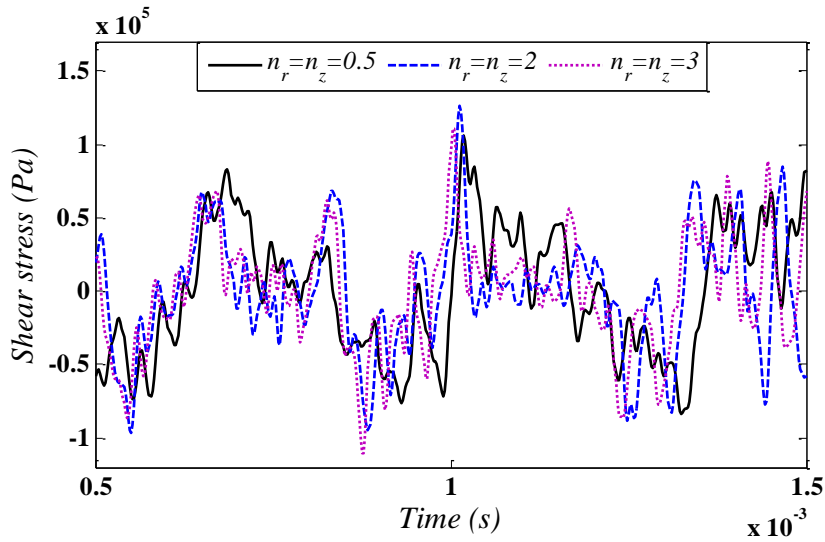


Figure 11: Time history of the shear stress ($\sigma_{r\theta}$) at $r = 0.3\text{ m}$, $\theta = 30^\circ$, $z = 0.25\text{ m}$ with $\beta = \pi/3$ for different values of n_r and n_z

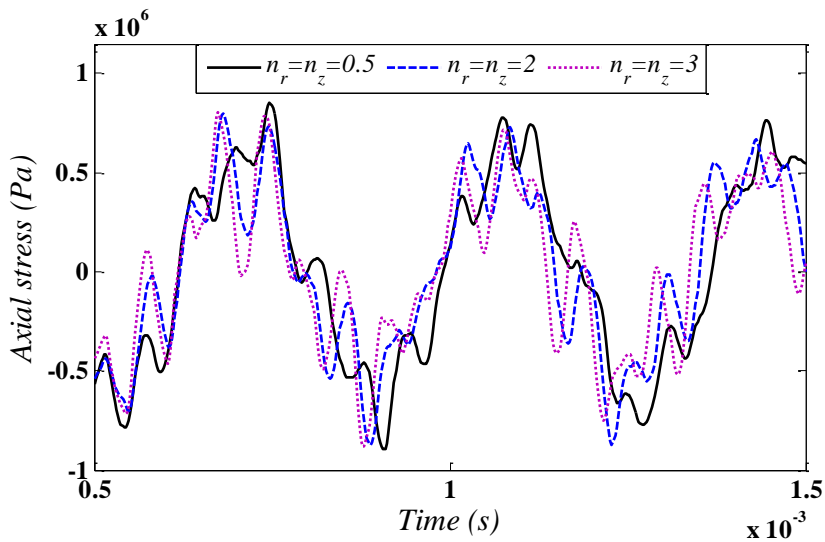


Figure 12: Time history of the axial stress at $r = 0.3\text{ m}$, $\theta = 30^\circ$, $z = 0.25\text{ m}$ with $\beta = \pi/3$ for different values of n_r and n_z

Figures 13 and 14 illustrate the time history of the radial displacement and stress at $r = 0.3\text{ m}$, $\theta = 30^\circ$, $z = 0.25\text{ m}$, respectively after the unloading for different values of β with power law exponents of $n_r = 2$, $n_z = 1$. It can be seen that by increasing the span angle of cylindrical panel, the amplitude of radial displacement is decreased while the frequency of vibration is increased.

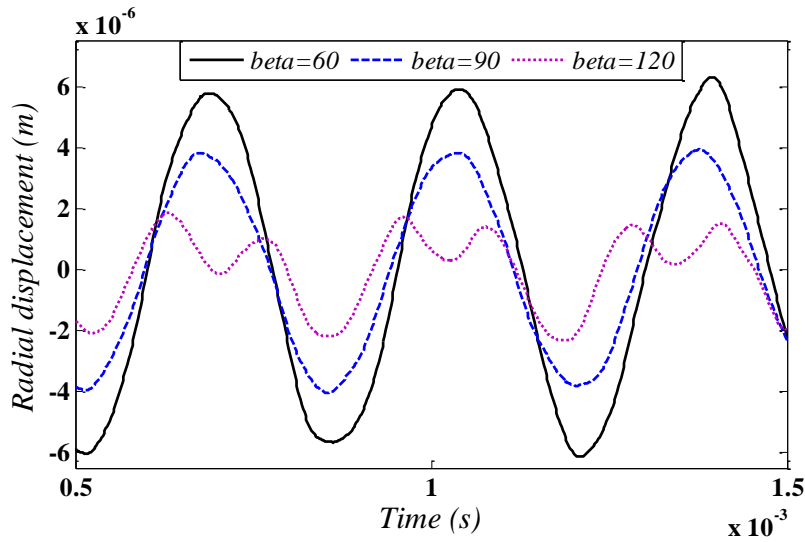


Figure 13: Time history of the radial displacement at $r = 0.3 \text{ m}$, $\theta = 30^\circ$, $z = 0.25 \text{ m}$ with $n_r = 2$, $n_z = 1$ for different values of β

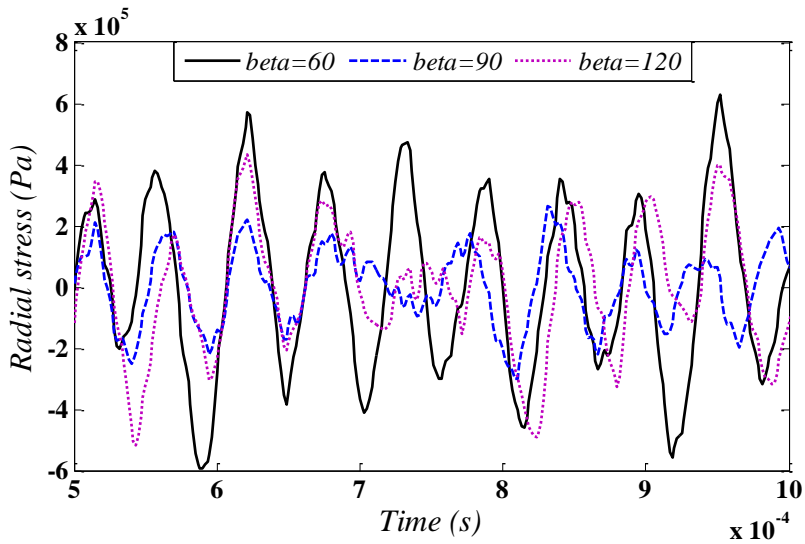


Figure 14: Time history of the radial stress at $r = 0.3 \text{ m}$, $\theta = 30^\circ$, $z = 0.25 \text{ m}$ with $n_r = 2$, $n_z = 1$ for different values of β

From the time history of the radial stress, it is possible to extract the approximate radial stress wave propagation velocity. Thus, by computing the time taken by the wave to cover the whole of the cylinder immediately after the loading, the approximate radial stress wave propagation velocities can be estimated. Table 3 shows the comparison of radial stress wave propagation velocity with analytical results (Jones, 1997) for cylindrical panels made of different homogenous materials. As it is obvious from this table, the obtained results have a good compatibility with analyti-

cal ones. Table 4 illustrates the variation of radial stress wave propagation velocity at different heights of cylindrical panel for different values of power law exponents. This table denotes that velocity of radial stress wave is strongly affected by the power law exponents. Also due to the variation of material properties through the axial direction, the velocity of radial stress wave at different heights of the cylindrical panel is changing.

	Material	Present (m/s)	Analytical (m/s)	Difference (%)
$n_r = 0, n_z = \infty$	$m1$	5714	5668	0.8
$n_r = n_z = 0$	$m2$	5970	5900	1.2
$n_r = n_z = \infty$	$c1$	7272	7189.8	1.1
$n_r = \infty, n_z = 0$	$c2$	8163	8231.4	0.8

Table 3: Comparison of radial stress wave propagation velocity of homogenous cylindrical panel with analytical results (Jones, 1997)

	$z = L/4$	$z = L/2$	$z = 3L/4$
$n_r = n_z = 0.5$	6504	6612	6723
$n_r = n_z = 3$	6897	6957	7143
$n_r = 3, n_z = 0$	7619	7619	7619
$n_r = 0, n_z = 3$	5797	5839	5882

Table 4: Velocity of radial stress wave propagation at different heights of cylindrical panel for different values of power law exponents

Now by introducing the normalized natural frequency as:

$$\Omega = 10\omega b \sqrt{\rho_{m1}/E_{m1}} \tag{41}$$

the fundamental normalized natural frequency of 2D-FG cylindrical panel for different values of the power law exponents and span angles are presented.

The effect of power law exponents on the fundamental normalized natural frequency (Ω) of 2D-FG cylindrical panel with $\beta = \pi/3$ is shown in Table 5. As it can be seen, by increasing n_r and decreasing n_z the fundamental normalized natural frequency increases.

	$n_r = 0$			$n_r = 1$			$n_r = 3$		
	$n_z = 0$	$n_z = 1$	$n_z = 3$	$n_z = 0$	$n_z = 1$	$n_z = 3$	$n_z = 0$	$n_z = 1$	$n_z = 3$
Ω	1.9871	1.9354	1.8639	2.3913	2.2569	2.1522	2.5700	2.3984	2.2786

Table 5: Fundamental normalized natural frequency for different values of power law exponents with $\beta = \pi/3$

Table 6 illustrates the effect of span angle of the 2D-FG cylindrical panel on the fundamental normalized natural frequency with $n_r = 2$ and $n_z = 1$. It is obvious that by increasing the span angle of cylindrical panel, the fundamental natural frequency grows.

	β					
	$\pi/12$	$\pi/6$	$\pi/4$	$\pi/3$	$\pi/2$	$2\pi/3$
Ω	1.5785	2.1792	2.3481	2.3515	2.3817	2.4318

Table 6: Fundamental normalized natural frequency for different values of span angle with $n_r = 2$, $n_z = 1$

Results denote that the distribution of displacements and stresses and natural frequencies are strongly affected by the power law exponents and the span angle of cylindrical panel. As it can be seen from the results, the distribution of stresses has continuous variations due to using graded elements. The use of GFEM has several benefits over the use of conventional FEM in the dynamic and wave propagation analyses. In conventional FEM, the boundary of homogenous elements of an inhomogeneous material acts as discrete boundaries for the stress waves. These boundaries cause artificial wave reflections and have a cumulative effect on the magnitude and speed of propagating stress waves. In addition, these inaccuracies will be more significant in 2D-FGM problems. Therefore, by using graded finite element in which the material property is graded continuously through the elements, accuracy can be improved without refining the mesh size.

4 CONCLUSIONS

The main purpose of the present paper is to study the 3D transient and free vibrational behaviour of 2D-FG cylindrical panels. The 3D graded finite element method and Rayleigh-Ritz energy formulation is applied. The proposed method is validated by the result of a 1D-FG thick hollow cylinder under the impact loading and an FG curved panel which are extracted from published literature. The comparisons between the results show that the present method has a good agreement with the existing results. Different types of displacement and stress in three directions and fundamental normalized natural frequency are presented for various values of power law exponents and span angle of cylindrical panel. Also, velocity of radial stress wave propagation for different power law exponents is obtained. Results denote that the maximum stresses, stress distribution, natural frequency and velocities of radial stress wave can be controlled by the variation of material properties in two directions. Based on the achieved results, 2D-FGMs have powerful potentials for designing and optimizing structures under multi-functional requirements.

References

- Akbarzadeh, A.H., Abbasi, M., Hosseini zad, S.K., Eslami, M.R. (2011). Dynamic analysis of functionally graded plates using the hybrid Fourier-Laplace transform under thermomechanical loading. *Meccanica* 46:1373-1392.
- Asemi, K., Salehi, M., Akhlaghi, M. (2010). Dynamic analysis of functionally graded thick truncated cone. *International Journal of Mechanics and Materials in design* 6:367-378.

- Asemi, K., Akhlaghi, M., Salehi, M. (2011). Dynamic analysis of thick short length FGM cylinders. *Meccanica* 47:1441-1453.
- Asgari, M., Akhlaghi, M., Hosseini, S.M. (2009). Dynamic analysis of two-dimensional functionally graded thick hollow cylinder with finite length under impact loading. *Acta Mechanica* 208:163-180.
- Asgari, M., Akhlaghi, M. (2010) Transient thermal stresses in two-dimensional functionally graded thick hollow cylinder with finite length. *Archive of Applied Mechanics* 80:353-376.
- Ashrafi, H., Asemi, K., Shariyat, M., Salehi, M. (2012) Two-dimensional modeling of heterogeneous structures using graded finite element and boundary element methods. *Meccanica* 48:663-680.
- Bahtui, A., Eslami, M.R. (2007) Coupled thermoelasticity of functionally graded cylindrical shells. *Mechanics Research Communications* 34:1-18.
- Birman, V., Byrd, L. (2007) Modeling and analysis of functionally graded materials and structures. *Applied Mechanics Reviews* 60:195-216.
- Bodaghi, M., Shakeri, M. (2012) An analytical approach for free vibration and transient response of functionally graded piezoelectric cylindrical panels subjected to impulsive loads. *Composite Structures* 94:1721-1735.
- Davar, A., Khalili, S.M.R., Malekzadeh Fard, K. (2013) Dynamic response of functionally graded circular cylindrical shells subjected to radial impulse load. *International Journal of Mechanics and Materials in Design* 9:65-81.
- Ebrahimi, M.J., Najafizadeh, M.M. (2014) Free vibration analysis of two-dimensional functionally graded cylindrical shells. *Applied Mathematical Modelling* 38: 308-324.
- Hosseini, M., Akhlaghi, M., Shakeri, M. (2007) Dynamic response and radial wave propagations of functionally graded thick hollow cylinder. *International Journal for Computer-Aided Engineering and Software* 24:288-303.
- Jha, D.K., Kant, T., Singh, R.K. (2013) A critical review of recent research on functionally graded plates. *Composite Structures* 96:833-849.
- Jones, N. (1997) *Structural Impact*. University Press, Cambridge.
- Kim, J.H., Paulino, G.H. (2002) Isoparametric graded finite elements for nonhomogeneous isotropic and orthotropic materials. *Journal of Applied Mechanics* 69:502-514.
- Koizumi, M. (1993) The concept of FGM. *Ceramic Transactions, Functionally Gradient Materials* 34:3-10.
- Malekzadeh, P., Monajjemzadeh, S.M. (2013) Dynamic response of functionally graded plates in thermal environment under moving load. *Composites Part B: Engineering* 45:1521-1533.
- Nemat-Alla, M. (2009) Reduction of thermal stresses by composition optimization of two-dimensional functionally graded materials. *Acta Mechanica* 208:147-161.
- Qian, L.F., Batra, R.C., Chen, L.M. (2004) Static and dynamic deformations of thick functionally graded elastic plates by using higher-order shear and normal deformable plate theory and meshless local Petrov-Galerkin method. *Composites Part B: Engineering* 35:685-697.
- Qu, Y., Long, X., Yuan, G., Meng, G. (2013) A unified formulation for vibration analysis of functionally graded shells of revolution with arbitrary boundary conditions. *Composites: Part B* 50: 381-402.
- Shakeri, M., Akhlaghi, M., Hosseini, S.M. (2006) Vibration and radial wave propagation velocity in functionally graded thick hollow cylinder. *Composite Structures* 76:174-181.
- Shao, Z.S., Fan, L.F., Wang, T.J. (2004) Analytical solutions of stresses in functionally graded circular hollow cylinder with finite length. *Key Engineering Materials* 261-263:651-656.
- Shao, Z.S. (2005) Mechanical and thermal stresses of a functionally graded circular hollow cylinder with finite length. *International Journal of Pressure Vessels and Piping* 82:155-163.
- Sun, D., Luo, S.N. (2011) The wave propagation and dynamic response of rectangular functionally graded material plates with completed clamped supports under impulse load. *European Journal of Mechanics A/Solids* 30:396-408.

Uymaz, B., Aydogdu, M. Three-Dimensional Vibration Analyses of Functionally Graded Plates under Various Boundary Conditions. *Journal of Reinforce Plastic Composites* 26:1847–1863.

Wang, X., Sudak, L.J. (2008) Three-dimensional analysis of multi-layered functionally graded anisotropic cylindrical panel under thermomechanical loading. *Mechanics of Materials* 40:235-254.

Yas, M.H., Sobhani Aragh B. (2010) Three-dimensional analysis for thermoelastic response of functionally graded fiber reinforced cylindrical panel. *Composite Structures* 92:2391-2399.

Zafarmand, H., Kadkhodayan, M. (2014) Three-dimensional static analysis of thick functionally graded plates using graded finite element method. *Proceedings of the Institution of Mechanical Engineers, Part C: Journal of Mechanical Engineering Science* 228:1275-1285.

Zafarmand, H., Hassani, B. (2014) Analysis of two-dimensional functionally graded rotating disks with variable thickness. *Acta Mechanica* 225:453–464.

Zahedinejad, P., Malekzadeh, P., Farid, M., Karami, G. (2010) A semi-analytical three-dimensional free vibration analysis of functionally graded curved panels. *International Journal of Pressure Vessels and Piping* 87:470-480.

Zienkiewicz, O.C., Taylor, R.L. (2005) *The finite element method for solid and structural mechanics*, 6th edn. Elsevier Butterworth-Heinemann, Oxford.

Appendix

The components of Φ are:

$$\Phi_i = \frac{1}{V} \Gamma \mathbf{X} \tag{A1}$$

where V is the volume of each element that is:

$$V = \begin{vmatrix} 1 & \xi_1 & \eta_1 & \zeta_1 & \xi_1\eta_1 & \xi_1\zeta_1 & \eta_1\zeta_1 & \xi_1\eta_1\zeta_1 \\ 1 & \xi_2 & \eta_2 & \zeta_2 & \xi_2\eta_2 & \xi_2\zeta_2 & \eta_2\zeta_2 & \xi_2\eta_2\zeta_2 \\ 1 & \xi_3 & \eta_3 & \zeta_3 & \xi_3\eta_3 & \xi_3\zeta_3 & \eta_3\zeta_3 & \xi_3\eta_3\zeta_3 \\ 1 & \xi_4 & \eta_4 & \zeta_4 & \xi_4\eta_4 & \xi_4\zeta_4 & \eta_4\zeta_4 & \xi_4\eta_4\zeta_4 \\ 1 & \xi_5 & \eta_5 & \zeta_5 & \xi_5\eta_5 & \xi_5\zeta_5 & \eta_5\zeta_5 & \xi_5\eta_5\zeta_5 \\ 1 & \xi_6 & \eta_6 & \zeta_6 & \xi_6\eta_6 & \xi_6\zeta_6 & \eta_6\zeta_6 & \xi_6\eta_6\zeta_6 \\ 1 & \xi_7 & \eta_7 & \zeta_7 & \xi_7\eta_7 & \xi_7\zeta_7 & \eta_7\zeta_7 & \xi_7\eta_7\zeta_7 \\ 1 & \xi_8 & \eta_8 & \zeta_8 & \xi_8\eta_8 & \xi_8\zeta_8 & \eta_8\zeta_8 & \xi_8\eta_8\zeta_8 \end{vmatrix} \tag{A2}$$

and:

$$\Gamma_{ij} = (-1)^{i+j} |A_{ij}| \tag{A3}$$

$$\mathbf{X} = \{1, \xi, \eta, \zeta, \xi\eta, \xi\zeta, \eta\zeta, \xi\eta\zeta\}^T \tag{A4}$$

in which:

$$\xi = r \cos \theta, \quad \eta = r \sin \theta, \quad \zeta = z \tag{A5}$$

$$\xi_i = r_i \cos \theta_i, \quad \eta_i = r_i \sin \theta_i, \quad \zeta_i = z_i \tag{A6}$$

where r_i , θ_i and z_i are nodal coordinates and A_{ij} is obtained from eliminating the i^{th} row and j^{th} column of V .